J Intell Robot Syst (2012) 68:53–68
DOI 10.1007/s10846-012-9665-x

Aerodynamic Modelling and Experimental Identification of a Coaxial-Rotor UAV

Arnaud Koehl · Hugues Rafaralahy · Mohamed Boutayeb · Bastien Martinez

Received: 9 September 2011 / Accepted: 29 February 2012 / Published online: 15 March 2012

Abstract A comprehensive design of a Gun Launched Micro Air Vehicle (GLMAV) is presented. The GLMAV rotorcraft is a new Micro Air Vehicle (MAV) concept using two-bladed coaxial contra-rotating rotors and a cyclic swashplate. The MAV packaged in a projectile is launched using the energy delivered by a portable weapon. When it reaches the apogee, the projectile is transformed in such a way that the MAV becomes operational over the zone to be observed. A detailed GLMAV nonlinear mathematical model is presented for hover and near-hover flight conditions and identified from experimental load data using a strain-gage aerodynamic balance. Simplifications brought to the aerodynamic submodel have permitted its linearization in the parameter space. The parameter estimation was based on the Kalman filter estimation method applied to the simplified aerodynamic model and using the input-output data from the experiment. The persistently exciting condition is given in terms of physical variables of the GLMAV through two simple expressions. The identification results are presented and validated through comparisons between the model output and real load data.

Keywords Unmanned aerial vehicles · System identification · Aerospace engineering · Nonlinear dynamical systems · Aerospace simulation · Process design

A. Koehl · B. Martinez
French-German Research Institute of Saint-Louis, 5 rue du Général Cassagnou, 68300, Saint-Louis, France

B. Martinez
e-mail: Bastien.Martinez@isl.eu

A. Koehl (✉) · H. Rafaralahy · M. Boutayeb
Research Center for Automatic Control of Nancy, Nancy-Université, CNRS, 186 rue de Lorraine, 54400, Cosnes et Romain, France
e-mail: Arnaud.Koehl@uhp-nancy.fr

H. Rafaralahy
e-mail: Hugues.Rafaralahy@uhp-nancy.fr

M. Boutayeb
e-mail: Mohamed.Boutayeb@uhp-nancy.fr

1 Introduction

Research and developments related to Unmanned Micro Air Vehicles (UMAVs) have been the subject of growing interest over the last few years, motivated by the recent technological advances in the fields of actuator miniaturization and embedded electronics. Thus the design of efficient and low-cost UMAV systems with autonomous navigation capacity has become possible, providing new tools for both civilian and military applications over the next years. The UMAV main objective will be to extend the human vision beyond

the natural horizon, in order to accomplish risky missions in the place of humans and in confined environments. Therefore, the new required capabilities will be to combine the hover flight to investigate a specific item in cluttered spaces with the agressive flight at high speeds and accelerations to reach remote areas, for both indoor and outdoor flights.

The rotary-wing UMAV is presently a fully potential and promising solution to this dual requirement among the vast existing mechanical configurations described in the literature [1, 3–5, 7, 25] amidst the families of single-rotor, twin-rotor, quad-rotor or hybrid-rotorcraft configurations. The coaxial contra-rotating rotor architecture has been chosen here because it best fulfils the needs of the Gun Launched Micro Air Vehicle (GLMAV) project.

This project is a new UMAV concept initiated in December 2006 at the French-German Research Institute of Saint-Louis as part of an innovative research activity. The GLMAV concept consists of bringing an MAV very quickly onto the site where it begins to be operational by using the energy delivered by an external device. Thereby, the embedded energy is maintained for the autonomous flight only. The principle illustrated in Fig. 1 is divided into three phases of flight: in the first one, the MAV packaged in the projectile shell is launched by a portable weapon and follows a ballistic trajectory to its apogee; in the second phase of flight, the projectile is transformed into an MAV where the rotor is deployed; the MAV can finally fulfill its mission in autonomous flight mode and then return to its launching area. It will be equipped with an autopilot ensuring the autonomous flight mode by generating good input signals to the various actuators and by using an INS [26] including low-cost sensors. The MAV will also be equipped with both daytime and night-vision systems, in order to observe the area of interest, which will also be useful in facilitating a future decision-making capacity.

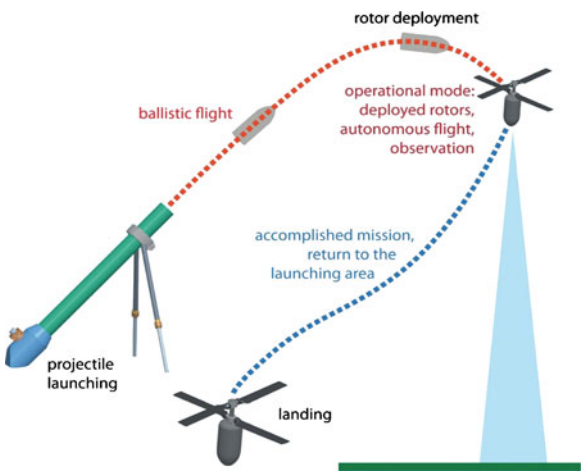

Fig. 1 GLMAV concept

Previous studies [9, 10, 23, 28] have demonstrated the GLMAV concept feasibility based on theoretical and experimental investigations concerning: the sizing of the device; its payload and autonomy; the necessary energy to launch the projectile containing the MAV; and the dimensioning of the portable weapon. These studies have also justified the choice of the two-bladed coaxial contra-rotating rotor aeromechanical configuration with a cyclic swashplate, which offers both advantages and disadvantages. The main criterion that favors this aeromechanical configuration over another is the compactness of folding which is critical to the conditioning of the MAV in the projectile shell. Other advantages lie in good maneuverability, good stability in hover and good forward speed capabilities. The coaxial contra-rotating rotors are also a compact anti-torque solution which prevents the MAV from rotating around its axis of rotation, and the payload is increased as both rotors participate in the thrust, compared to other conventional configurations with a single rotor. The vibrations on the MAV body and the aerodynamic interactions generated by the rotating blades constitute the main weakness of this coaxial rotor configuration which alter cruise and hover efficiency. More information about the coaxial rotor aeromechanical analysis could be found in the literature [7, 11, 21] and in other existing MAV projects [19, 20, 24, 27].

The flight dynamics of the UMAV with rotating wings is nonlinear and therefore complex. Thus, it is necessary to characterize the nonlinearities for each flight configuration in order to provide these devices with autonomous navigation capabilities. But conversely, the great variability of the parameters makes it impossible to compile a complete

GLMAV mathematical model which captures all the aerodynamic effects.

The main contribution of this paper is the construction and the experimental validation of the aerodynamic model of an MAV with coaxial rotors and a cyclic swashplate. The purpose is to identify the GLMAV model in the hover-flight case (i.e. with low body incidence angles and velocities). The GLMAV modeling is limited to the quasi-stationary flight mode. The body dynamics (i.e. the shell dynamics) is modeled like a rigid body with 6 Degrees of Freedom, supplemented by aerodynamic forces due to the rotor rotation and the swashplate incidence angles. The estimation of the unknown GLMAV model parameters is simplified by using the linearized aerodynamic model and experimental data (i.e. without the nonlinearity constraints from the six-DoF model). The model validation task finally demonstrates the good simulation capability of the constructed aerodynamic model.

In the present paper, Section 2 presents the nonlinear modeling of the new Gun Launched MAV concept with two-bladed coaxial contra-rotating rotors in the hover-flight case. Section 3 introduces an experimental method using a strain-gage aerodynamic balance to measure and then to collect the input-actuator data and the load data. In Section 4, the aerodynamic model is first simplified and linearized, then used with the data collected in Section 3 to estimate the aerodynamic parameters through the Kalman filter estimation method. Section 5 gives the validation results by comparing other sets of data than those used in Section 4 to the model output reconstructions.

2 MAV Modeling

This Section presents the GLMAV mathematical model built from the mechanical and aeromechanical physical laws. Early studies [10, 15, 16, 18, 19] show that miniature rotorcraft mathematical models can be divided into two sub-models (i.e. an aerodynamic model coupled with the generic 6-DoF model). Hence the main difficulty lies in the aerodynamic modeling which must be complete enough to accurately simulate the GLMAV dynamics block (see Fig. 2) and simple enough to develop future control laws for the hover-flight case and autonomous trajectory tracking.

2.1 6-DoF Model

The GLMAV is considered to be a rigid body with a fixed mass m. The following generic 6-DoF Equations refer to its motion in three-dimensional space. It describes the rotational and translational dynamics and kinematics using Newton's second law, the six aerodynamic loads $\mathbf{X}, \mathbf{Y}, \mathbf{Z}, \mathbf{L}, \mathbf{M}, \mathbf{N}$ and the motion-derived equations relative to the body-fixed reference frame (see [19, 25] and references therein for detailed explanations). Thus the translational kinematic is written as:

$$\begin{pmatrix}\dot{x}\\ \dot{y}\\ \dot{z}\end{pmatrix} = \begin{pmatrix} c_\theta c_\psi & s_\phi s_\theta c_\psi - c_\phi s_\psi & c_\phi s_\theta c_\psi + s_\phi s_\psi \\ c_\theta s_\psi & s_\phi s_\theta s_\psi + c_\phi c_\psi & c_\phi s_\theta s_\psi - s_\phi c_\psi \\ -s_\theta & s_\phi c_\theta & c_\phi c_\theta \end{pmatrix} \begin{pmatrix} u \\ v \\ w \end{pmatrix}, \tag{1}$$

where $c_\alpha = \cos\alpha$, $s_\alpha = \sin\alpha$, x, y, z are the three gravity-center position variables expressed in the body coordinate system $\{\mathrm{G}, \mathbf{x}_\mathrm{b}, \mathbf{y}_\mathrm{b}, \mathbf{z}_\mathrm{b}\}$, ϕ, θ, ψ are the Euler angles expressed in the Earth's coordinate system $\{\mathrm{O}, \mathbf{x}_\mathrm{e}, \mathbf{y}_\mathrm{e}, \mathbf{z}_\mathrm{e}\}$ and u, v, w are the three gravity center translational velocity variables expressed in the body coordinate system.

The rotational kinematics depends on the Euler angles and the three angular velocity variables p, q, r such that:

$$\begin{pmatrix}\dot{\phi}\\ \dot{\theta}\\ \dot{\psi}\end{pmatrix} = \begin{pmatrix} 1 & \tan\theta\sin\phi & \tan\theta\cos\phi \\ 0 & \cos\phi & -\sin\phi \\ 0 & \dfrac{\sin\phi}{\cos\theta} & \dfrac{\cos\phi}{\cos\theta} \end{pmatrix} \begin{pmatrix} p \\ q \\ r \end{pmatrix}. \tag{2}$$

The translational dynamic equation is written as:

$$m\begin{pmatrix}\dot{u}\\ \dot{v}\\ \dot{w}\end{pmatrix} = \begin{pmatrix} X \\ Y \\ Z \end{pmatrix} - m\begin{pmatrix} 0 & -r & q \\ r & 0 & -p \\ -q & p & 0 \end{pmatrix}\begin{pmatrix} u \\ v \\ w \end{pmatrix}. \tag{3}$$

Finally, the rotational dynamic equation is expressed as:

$$\mathbf{I}\begin{pmatrix}\dot{p}\\ \dot{q}\\ \dot{r}\end{pmatrix} = \begin{pmatrix} L \\ M \\ N \end{pmatrix} - \begin{pmatrix} 0 & -r & q \\ r & 0 & -p \\ -q & p & 0 \end{pmatrix}\mathbf{I}\begin{pmatrix} p \\ q \\ r \end{pmatrix}, \tag{4}$$

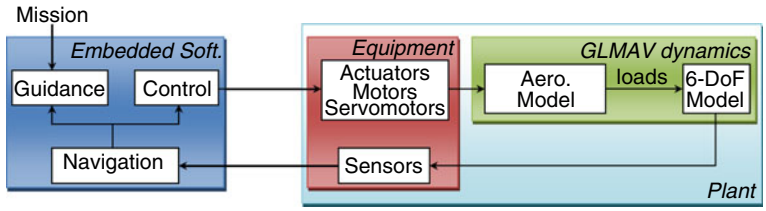

Fig. 2 Closed-loop GLMAV system block diagram

where the GLMAV inertial matrix $\mathbf{I}$ is approximated by:

$$\mathbf{I} = \begin{pmatrix} I_{xx} & 0 & 0 \\ 0 & I_{yy} & 0 \\ 0 & 0 & I_{zz} \end{pmatrix} \tag{5}$$

as the GLMAV is axisymmetric along $\mathbf{z}_\mathrm{b}$, implying that the non-diagonal elements of $\mathbf{I}$ can be approximated by zero. Furthermore, for the same reason as previously: $I_{xx} \cong I_{yy}$.

2.2 Aerodynamic Model

The aerodynamic model presented in the following is divided into the forces induced by the body immersed in the airflow and the loads generated by the coaxial rotors and the cyclic swashplate incidence angles. We neglect the gyroscopic moments induced by the contra-rotating rotors, as they offset one another, assuming that the speed differential is virtually zero or is not large enough to induce a significant gyroscopic moment, which is realistic in the hover-flight case (Fig. 3).

2.2.1 Forces Generated by the Coaxial Rotor

The thrust is the main force generated by both rotors allowing the GLMAV to control its rate of climb. The upper rotor contributes only to the vertical thrust $\mathbf{T}_1$ which is directly proportional to the upper rotor aerodynamic coefficient α and to the rotation speed Ω_1:

$$\mathbf{T}_1 = \begin{pmatrix} 0 \\ 0 \\ \alpha\Omega_1^2 \end{pmatrix}. \tag{6}$$

The lower rotor generates both a vertical thrust according to the $\mathbf{z}_\mathrm{b}$ base vector and two lateral forces due to the swashplate incidence angles according to the $\mathbf{x}_\mathrm{b}$ and $\mathbf{y}_\mathrm{b}$ base vectors. Thus for a given rotor-rotation speed, the vertical thrust is maximized if these angles are null; otherwise, the vertical thrust decreases due to the lateral force components being non-zero. The expression of the lower rotor forces $\mathbf{T}_2$ depends on the swashplate incidence angles $(\delta_{c_x}, \delta_{c_y})$, such that:

$$\mathbf{T}_2 = \mathbf{R}\left(\delta_{c_x}, \delta_{c_y}\right) \begin{pmatrix} 0 \\ 0 \\ \beta\Omega_2^2 \end{pmatrix}, \tag{7}$$

where

$$\mathbf{R}\left(\delta_{c_x}, \delta_{c_y}\right) = \begin{pmatrix} \cos\delta_{c_y} & -\sin\delta_{c_y}\sin\delta_{c_x} & -\sin\delta_{c_y}\cos\delta_{c_x} \\ 0 & \cos\delta_{c_x} & -\sin\delta_{c_x} \\ \sin\delta_{c_y} & \cos\delta_{c_y}\sin\delta_{c_x} & \cos\delta_{c_x}\cos\delta_{c_y} \end{pmatrix} \tag{8}$$

is a transformation matrix between the body and lower rotor coordinate systems $\{\mathrm{G}, \mathbf{x}_\mathrm{b}, \mathbf{y}_\mathrm{b}, \mathbf{z}_\mathrm{b}\}$ and $\{\mathrm{O}_2, \mathbf{x}_\mathrm{r}, \mathbf{y}_\mathrm{r}, \mathbf{z}_\mathrm{r}\}$, β is the rotor aerodynamic

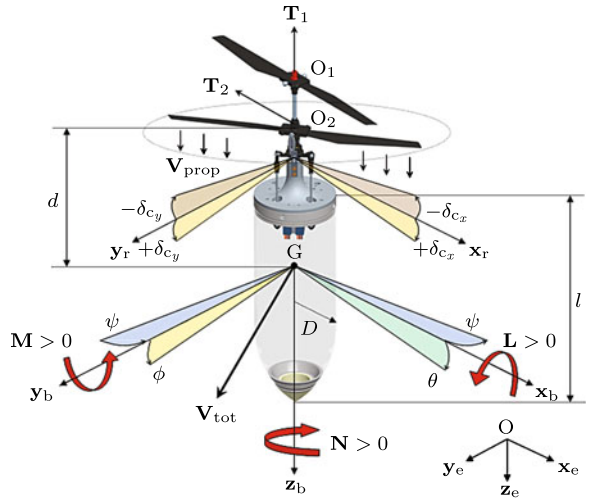

Fig. 3 GLMAV with a rotor articulated by cyclic a cyclic swashplate

coefficient and Ω_2 is the lower rotor-rotation speed. By computing Eqs. 7 and 8, the force $\mathbf{T}_2$ generated by the lower rotor is written as:

$$\mathbf{T}_2 = \beta\Omega_2^2 \begin{pmatrix} -\sin\delta_{c_y}\cos\delta_{c_x} \\ -\sin\delta_{c_x} \\ \cos\delta_{c_x}\cos\delta_{c_y} \end{pmatrix}. \tag{9}$$

In Eqs. 6 and 9, the developed expressions of the thrust aerodynamic coefficients α and β are a function of the original thrust coefficients C_{T_1} and C_{T_2}, of the Reynolds number R_E which characterizes the airflow regimes such as the laminar or turbulent flow, and of the air density ρ, such that:

$$\alpha \triangleq C_{T_1}\pi R_E^4\rho, \tag{10}$$

$$\beta \triangleq C_{T_2}\pi R_E^4\rho. \tag{11}$$

Given that each rotor thrust is known from Eqs. 6 and 9, the total thrust $\mathbf{T}$ according to $\mathbf{z}_b$ could be computed using the sum of the two individual rotor thrusts $[\mathbf{T_1}]_{\mathbf{z}_b}, [\mathbf{T}_2]_{\mathbf{z}_b}$. However, in practice, this thrust is lower than this sum as there is a loss of aerodynamic efficiency due to airflow interactions. The expression of the total useful thrust is:

$$[\mathbf{T}]_{\mathbf{z}_b} = \sigma\left(\alpha\Omega_1^2 + \beta\cos\delta_{c_x}\cos\delta_{c_y}\Omega_2^2\right), \tag{12}$$

where σ is a loss coefficient with $0.8 \lessapprox \sigma \lessapprox 1$.

Finally, the total force generated by the coaxial rotor is calculated from Eqs. 9 and 12, such that:

$$\mathbf{T} = \begin{pmatrix} -\beta\sin\delta_{c_y}\cos\delta_{c_x}\Omega_2^2 \\ -\beta\sin\delta_{c_x}\Omega_2^2 \\ \sigma\alpha\Omega_1^2 + \sigma\beta\cos\delta_{c_x}\cos\delta_{c_y}\Omega_2^2 \end{pmatrix}. \tag{13}$$

2.2.2 Total Wind Velocity

In order to determine the aerodynamic forces acting on the body, it is necessary to know both the direction and velocity of the total airflow inside which the GLMAV operates. In all, three main wind sources composing the total wind vector $\mathbf{V}_{tot}$ can be identified: the first component corresponds to the airflow speed $\mathbf{V}_{prop}$ generated by the coaxial rotors; the second component is $\mathbf{V}_{body}$ due to the airflow generated by the translational and rotational body displacements and finally a third component $\mathbf{V}_{wind}$ is due to the externally induced wind, in general unpredictable. The total wind vector in the body coordinate system is then written as:

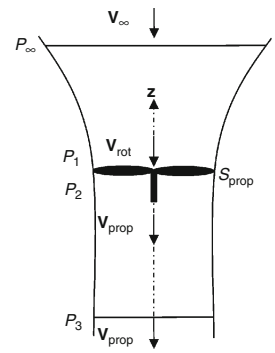

Fig. 4 Airflow profile generated by a single rotor

$$\mathbf{V}_{tot} = \mathbf{V}_{prop} - \mathbf{V}_{body} + \mathbf{V}_{wind}. \tag{14}$$

By considering only one rotating rotor, the wind velocity $\mathbf{V}_{prop}$ generated by the coaxial rotor blades can be modeled using Bernoulli's theorem. The latter illustrates the conservation of mechanical energy by considering a permanent airflow between points with corresponding pressures P_∞ and P_3 and by using the intermediate pressures P_1 and P_2, the airflow speed V_{rot} close to the rotor, the airflow speed to infinity V_∞ and the air density ρ according to Fig. 4:[1]

$$\frac{1}{2}\rho V_{rot}^2 + P_2 = \frac{1}{2}\rho V_{prop}^2 + P_3, \tag{15}$$

$$\frac{1}{2}\rho V_\infty^2 + P_\infty = \frac{1}{2}\rho V_{rot}^2 + P_1. \tag{16}$$

Equations 15 and 16 are valid if the fluid is assumed to be incompressible and perfect, given the low axial airflow velocities. Taking into account the fact that $V_\infty = 0$ and $P_\infty = P_3 = P_{atm}$ with P_{atm}, representing the atmospheric pressure, Eqs. 15 and 16 can be rewritten respectively as:

$$\frac{1}{2}\rho\left(V_{rot}^2 - V_{prop}^2\right) = P_{atm} - P_2, \tag{17}$$

$$P_{atm} - P_1 = \frac{1}{2}\rho V_{rot}^2. \tag{18}$$

[1] In the following we assume that the airflow circumferential velocity component added by the first rotor is cancelled out by the contra-rotating second one.

The thrust of the rotor $\mathbf{T}_\mathrm{r}$, according to the $\mathbf{z}$ base vector, is a function of the pressures P_1 and P_3 and of the rotor-disc surface S_prop, such that:

$$\mathbf{T}_\mathrm{r} = S_\mathrm{prop}\left(P_2 - P_1\right). \tag{19}$$

By manipulating Eqs. 17–19, the airflow speed generated by the rotor is written as:

$$\mathbf{V}_\mathrm{prop} = \sqrt{\frac{-2\mathbf{T}_\mathrm{r}}{\rho S_\mathrm{prop}}}. \tag{20}$$

By using Eqs. 12, 14 and 20 and assuming that $[\mathbf{T}]_{\mathbf{z}_\mathrm{b}} = \mathbf{T}_\mathrm{r}$, the expressions of the three components of the total wind $\mathbf{V}_\mathrm{tot}$ that are $\mathbf{V}_{ux}$, $\mathbf{V}_{vy}$ and $\mathbf{V}_{wz}$, are written as follows:

$$\mathbf{V}_{ux} = -u + [\mathbf{V}_\mathrm{wind}]_{\mathbf{x}_\mathrm{b}}, \tag{21}$$

$$\mathbf{V}_{vy} = -v + [\mathbf{V}_\mathrm{wind}]_{\mathbf{y}_\mathrm{b}}, \tag{22}$$

$$\mathbf{V}_{wz} = \sqrt{\frac{-2\sigma\left(\alpha\Omega_1^2 + \beta\cos\delta_{c_x}\cos\delta_{c_y}\Omega_2^2\right)}{\rho S_\mathrm{prop}}} - w + [\mathbf{V}_\mathrm{wind}]_{\mathbf{z}_\mathrm{b}}, \tag{23}$$

where $\alpha < 0$ and $\beta < 0$; u, v and w are the three translational body-velocity components of the GLMAV and $[\mathbf{V}_\mathrm{wind}]_{\mathbf{x}_\mathrm{b}}$, $[\mathbf{V}_\mathrm{wind}]_{\mathbf{y}_\mathrm{b}}$, and $[\mathbf{V}_\mathrm{wind}]_{\mathbf{z}_\mathrm{b}}$ are the three components of the wind vector $\mathbf{V}_\mathrm{wind}$.

2.2.3 Forces Acting on the Body

Given that the expression of $\mathbf{V}_\mathrm{tot}$ is known, the forces acting on the GLMAV body could be defined supposing that the body is composed of two elementary volumes: a cylinder and a half-sphere. The three force components of the body force $\mathbf{f}_\mathrm{body}$ depend on the air density ρ, the body length l and radius D, the projectile cylinder surface S_c according to the plane $\{\mathbf{x}_\mathrm{b}, \mathbf{z}_\mathrm{b}\}$, the section of the projectile cylinder S_s in which the coaxial rotor is conditioned, the body shape aerodynamic coefficients C_x, C_y and C_z, and the total wind velocity $\mathbf{V}_\mathrm{tot}$;

$$\begin{aligned}
[\mathbf{f}_\mathrm{body}]_{\mathbf{x}_\mathrm{b}} &= \frac{1}{2}\rho S_\mathrm{c} C_x \mathbf{V}_{ux}\|\mathbf{V}_\mathrm{tot}\|,\\
[\mathbf{f}_\mathrm{body}]_{\mathbf{y}_\mathrm{b}} &= \frac{1}{2}\rho S_\mathrm{c} C_y \mathbf{V}_{vy}\|\mathbf{V}_\mathrm{tot}\|,\\
[\mathbf{f}_\mathrm{body}]_{\mathbf{z}_\mathrm{b}} &= \frac{1}{2}\rho S_\mathrm{s} C_z \mathbf{V}_{wz}\|\mathbf{V}_\mathrm{tot}\|,
\end{aligned} \tag{24}$$

where

$$\|\mathbf{V}_\mathrm{tot}\| = \sqrt{\mathbf{V}_{ux}^2 + \mathbf{V}_{vy}^2 + \mathbf{V}_{wz}^2} \tag{25}$$

and

$$\begin{aligned}
S_\mathrm{c} &= 2Dl,\\
S_\mathrm{s} &= \pi D^2.
\end{aligned} \tag{26}$$

The weight force component $\mathbf{f}_\mathrm{p}$ acting on the GLMAV is written as:

$$\mathbf{f}_\mathrm{p} = mg\begin{pmatrix} -\sin\theta \\ \cos\theta\sin\phi \\ \cos\theta\cos\phi \end{pmatrix}. \tag{27}$$

Finally, the three components $\mathbf{X}$, $\mathbf{Y}$ and $\mathbf{Z}$ of the total force vector $\mathbf{f}_\mathrm{tot}$ applied to the GLMAV represent the sum of the coaxial rotor, body and gravity force vectors:

$$\mathbf{f}_\mathrm{tot} = \begin{pmatrix} \mathbf{X} \\ \mathbf{Y} \\ \mathbf{Z} \end{pmatrix} = \mathbf{T} + \mathbf{f}_\mathrm{body} + \mathbf{f}_\mathrm{p}. \tag{28}$$

2.2.4 Moments Induced by Both Rotors

By knowing the total force vector, the resulting total moment can be computed and thus the aerodynamic model can be completed. In order to simplify and to reduce the model complexity, it is assumed that the forces generated by the body immersed in the airflow induce a negligible moment. This is due to the fact that the wind velocity from the coaxial rotors is far greater than the one produced by the body and the external wind, i.e.:

$$\mathbf{V}_\mathrm{prop} \gg \mathbf{V}_\mathrm{body} \quad \text{and} \quad \mathbf{V}_\mathrm{prop} \gg \mathbf{V}_\mathrm{wind}. \tag{29}$$

Consequently, the lateral force components $[\mathbf{f}_\mathrm{body}]_{\mathbf{x}_\mathrm{b}}$ and $[\mathbf{f}_\mathrm{body}]_{\mathbf{y}_\mathrm{b}}$ are negligible compared to $[\mathbf{f}_\mathrm{body}]_{\mathbf{z}_\mathrm{b}}$. In addition, a strong gust of wind would only be regarded as a force acting on the whole GLMAV body because of its small dimensions; thus only the forces generated by the rotors could lead to a non-zero resulting moment. The pitch and roll moments $\mathbf{M}$, $\mathbf{L}$ induced by the incidence angles of the lower rotor are calculated using the cross product of the distance vector from the gravity center to the rotor-rotation center GO_2 with the lower-rotor thrust vector:

$$\begin{pmatrix} \mathbf{L} \\ \mathbf{M} \end{pmatrix} = \mathrm{GO}_2 \wedge \mathbf{T}_2. \tag{30}$$

By calculating Eq. 30, both the lateral moment components **L** and **M** are written as:

$$\mathbf{L} = -d\beta \sin\delta_{c_x}\Omega_2^2, \tag{31}$$

$$\mathbf{M} = d\beta \sin\delta_{c_y}\cos\delta_{c_x}\Omega_2^2, \tag{32}$$

where d is the distance between the points G and O_2.

Finally, the yaw moment **N** generated by each rotor is directly proportional to their respective aerodynamic coefficients γ_1, γ_2 and rotation speeds Ω_1, Ω_2:

$$\mathbf{N} = \gamma_1\Omega_1^2 + \gamma_2\Omega_2^2. \tag{33}$$

2.3 Complete GLMAV Model

The complete nonlinear GLMAV model in the hover-flight case (i.e. considering small translational displacements with small body incidence angles and velocities) is described by computing Eqs. 1–4, 13, 21–28 and 31–33:

The developed translational kinematic equations are written as:

$$\dot{x} = (\cos\theta\cos\psi)u + (\sin\phi\sin\theta\cos\psi - \cos\phi\sin\psi)v + (\cos\phi\sin\theta\cos\psi + \sin\phi\sin\psi)w, \tag{34}$$

$$\dot{y} = (\cos\theta\sin\psi)u + (\sin\phi\sin\theta\sin\psi + \cos\phi\cos\psi)v + (\cos\phi\sin\theta\sin\psi - \sin\phi\cos\psi)w, \tag{35}$$

$$\dot{z} = (-\sin\theta)u + (\sin\phi\cos\theta)v + (\cos\phi\cos\theta)w; \tag{36}$$

the developed rotational kinematic equations are expressed as:

$$\dot{\phi} = p + (\tan\theta\sin\phi)q + (\tan\theta\cos\phi)r, \tag{37}$$

$$\dot{\theta} = (\cos\phi)q - (\sin\phi)r, \tag{38}$$

$$\dot{\psi} = \left(\frac{\sin\phi}{\cos\theta}\right)q + \left(\frac{\cos\phi}{\cos\theta}\right)r; \tag{39}$$

the complete translational dynamic equations are written as:

$$\dot{u} = rv - qw - \frac{\beta}{m}\sin\delta_{c_y}\cos\delta_{c_x}\Omega_2^2 - \frac{1}{2m}\rho S_c C_x \mathbf{V}_{ux}\sqrt{\mathbf{V}_{ux}^2 + \mathbf{V}_{vy}^2 + \mathbf{V}_{wz}^2} - g\sin\theta, \tag{40}$$

$$\dot{v} = pw - ru - \frac{\beta}{m}\sin\delta_{c_x}\Omega_2^2 - \frac{1}{2m}\rho S_c C_y \mathbf{V}_{vy}\sqrt{\mathbf{V}_{ux}^2 + \mathbf{V}_{vy}^2 + \mathbf{V}_{wz}^2} + g\cos\theta\sin\phi, \tag{41}$$

$$\dot{w} = qu - pv + \frac{\sigma}{m}\alpha\Omega_1^2 + \frac{\sigma}{m}\beta\cos\delta_{c_x}\cos\delta_{c_y}\Omega_2^2 + \frac{1}{2m}\rho S_s C_z \mathbf{V}_{wz}\sqrt{\mathbf{V}_{ux}^2 + \mathbf{V}_{vy}^2 + \mathbf{V}_{wz}^2} + g\cos\theta\cos\phi\Big), \tag{42}$$

where

$$\mathbf{V}_{ux} = -u + [\mathbf{V}_{\text{wind}}]_{\mathbf{x}_b}, \tag{43}$$

$$\mathbf{V}_{vy} = -v + [\mathbf{V}_{\text{wind}}]_{\mathbf{y}_b}, \tag{44}$$

$$\mathbf{V}_{wz} = [\mathbf{V}_{\text{prop}}]_{\mathbf{z}_b} - w + [\mathbf{V}_{\text{wind}}]_{\mathbf{z}_b}, \tag{45}$$

$$[\mathbf{V}_{\text{prop}}]_{\mathbf{z}_b} = \sqrt{\frac{-2\sigma\left(\alpha\Omega_1^2 + \beta\cos\delta_{c_x}\cos\delta_{c_y}\Omega_2^2\right)}{\rho S_{\text{prop}}}}. \tag{46}$$

Finally, the complete rotational dynamic equations are written as:

$$\dot{p} = \left(\frac{I_{yy} - I_{zz}}{I_{xx}}\right)rq - \frac{1}{I_{xx}}\left(d\beta\sin\delta_{c_x}\Omega_2^2\right), \tag{47}$$

$$\dot{q} = \left(\frac{I_{zz} - I_{xx}}{I_{yy}}\right)rp + \frac{1}{I_{yy}}\left(d\beta\sin\delta_{c_y}\cos\delta_{c_x}\Omega_2^2\right), \tag{48}$$

$$\dot{r} = \left(\frac{I_{xx} - I_{yy}}{I_{zz}}\right)pq + \frac{1}{I_{zz}}\left(\gamma_1\Omega_1^2 + \gamma_2\Omega_2^2\right). \tag{49}$$

3 Experimental Design

The previous Section presented a GLMAV mathematical model for the hover and near-hover

Fig. 5 Six-component strain-gage aerodynamic balance

flight cases. From this point onward, the experimental purpose is to measure the loads according to the rotor-rotation speeds and to the cyclic swashplate incidence angles defined as input data. The complete nonlinear model structure described by Eqs. 34–49 is complex and therefore difficult to apply to the task of estimating the aerodynamic parameter values. Furthermore, the entire GLMAV model (i.e. aerodynamic and 6-DoF models) requires the ability to measure the 6-DoF model output from an in-flight MAV with its active embedded electronics.

However, we noticed that all the parameter values required could be estimated by only considering the aerodynamic submodel. The main advantage is that the aerodynamic model can be quite easily linearized in the parameter space. Therefore, well-known and simple linear estimation techniques could be applied to our problem of estimating aerodynamic parameters, which will be addressed in the next Section. The 6 load components X, Y, Z, L, M and N are also the required output data which are easy to measure by means of static experiments (i.e. without using a flying MAV). The 6 load components were measured using a strain-gage aerodynamic balance illustrated in Fig. 5. The MAV shown in Fig. 6a was rigidly fixed to the aerodynamic balance which was also fastened to a supporting base, as shown in Fig. 6b. The Bell–Hiller stabilizer bar displayed in Fig. 6a was not used as it was useless for static experiments. Previous studies [2, 6] explained the useful dynamic effects of the Bell–Hiller bar. The MAV mechanical design was inspired by the ready-to-fly model kit and was made from both purchased and ISL-designed components. The total MAV weight was of about 250 g, including the lithium-polymer battery pack and the future active embedded electronics, the MAV was 30 cm high and the lower/upper rotor diameter was of 34 cm. As determined by the experiments, the total thrust of the coaxial rotor was of about 300 g, leaving a payload of 50 g.

Figure 7 illustrates the complete and practical measurement process of collecting the output data according to the generated input signals. At each step in time, both motor and servomotor numerical input values were generated through a dedicated program, then numerical input signals were converted into adapted PWM signals and routed to the four actuators via a demultiplexer and a transmitter interface. At the same time,

(a) (b)

Fig. 6 **a** GLMAV archetype—**b** aerodynamic balance on its supporting base

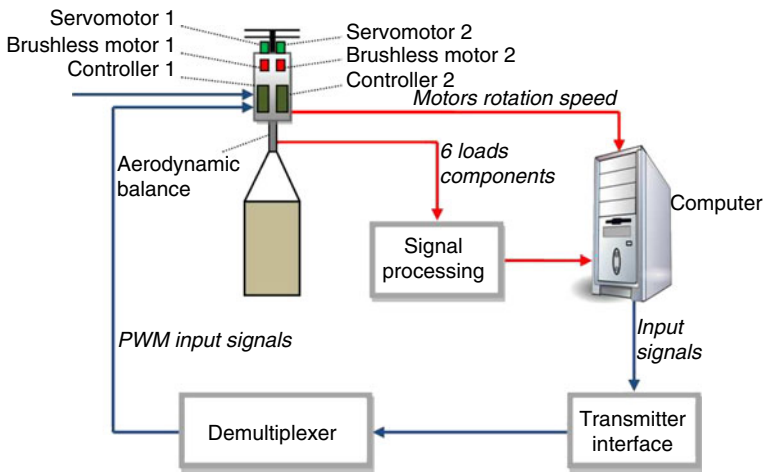

Fig. 7 Experimental design diagram

the output load data from the aerodynamic balance were measured and transformed into useful numerical values by means of signal processing electronics and then saved. Knowing that the strain-gage sensor dynamics exceeded the actuator dynamics (i.e. both motors and servomotors), it was assumed that the aerodynamic strain-gage balance response was instantaneous.

To conclude this Section, some remarks can be made about the measurement process:

- The generated motor input signals were not reliable as input data; therefore the motor speeds considered were measured through optical sensors;
- The MAV was fixed to the aerodynamic balance so that their coordinate systems were oriented in the same directions;
- The whole MAV aerodynamic balance had to be sufficiently distant from the floor and walls to avoid disturbing the coaxial rotor aerodynamic airflow, which would have resulted in ground effects measurements;
- The measurements of the X and Y forces were only used to validate the model in Section 5, since all the aerodynamic parameters could be estimated only by measuring the Z, L, M, and N loads.

4 Parameter Estimation

Given that the aerodynamic model and input-output data are known, the aerodynamic parameters can be estimated. To simplify the estimation problem, the aerodynamic model is linearized in the parameter space. By computing Eqs. 13, 21–28, and 31–33, the nonlinear aerodynamic model is written as follows:

$$X = -\beta \sin\delta_{c_y} \cos\delta_{c_x} \Omega_2^2 - \frac{1}{2}\rho S_c C_x \mathbf{V}_{ux} \sqrt{\mathbf{V}_{ux}^2 + \mathbf{V}_{vy}^2 + \mathbf{V}_{wz}^2} - mg\sin\theta, \tag{50}$$

$$Y = -\beta \sin\delta_{c_x} \Omega_2^2 - \frac{1}{2}\rho S_c C_y \mathbf{V}_{vy} \sqrt{\mathbf{V}_{ux}^2 + \mathbf{V}_{vy}^2 + \mathbf{V}_{wz}^2} + mg\cos\theta\sin\phi, \tag{51}$$

$$Z = \sigma\alpha\Omega_1^2 + \sigma\beta\cos\delta_{c_x}\cos\delta_{c_y}\Omega_2^2 + \frac{1}{2}\rho S_s C_z \mathbf{V}_{wz} \sqrt{\mathbf{V}_{ux}^2 + \mathbf{V}_{vy}^2 + \mathbf{V}_{wz}^2} + mg\cos\theta\cos\phi, \tag{52}$$

where

$$\mathbf{V}_{ux} = -u + [\mathbf{V}_{\text{wind}}]_{\mathbf{x}_b}, \tag{53}$$

$$\mathbf{V}_{vy} = -v + [\mathbf{V}_{\text{wind}}]_{\mathbf{y}_b}, \tag{54}$$

$$\mathbf{V}_{wz} = [\mathbf{V}_{\text{prop}}]_{\mathbf{z}_b} - w + [\mathbf{V}_{\text{wind}}]_{\mathbf{z}_b}, \tag{55}$$

$$[\mathbf{V}_{\text{prop}}]_{\mathbf{z}_b} = \sqrt{\frac{-2\sigma\left(\alpha\Omega_1^2 + \beta\cos\delta_{c_x}\cos\delta_{c_y}\Omega_2^2\right)}{\rho S_{\text{prop}}}}, \tag{56}$$

and

$$L = -d\beta \sin \delta_{c_x} \Omega_2^2, \tag{57}$$

$$M = d\beta \sin \delta_{c_y} \cos \delta_{c_x} \Omega_2^2, \tag{58}$$

$$N = \gamma_1 \Omega_1^2 + \gamma_2 \Omega_2^2. \tag{59}$$

The nonlinear model consisting of Eqs. 50–59 could be simplified. Indeed, in the first place it is obvious that the gravity-center translational velocities u, v, w are zero, since the MAV is rigidly fixed to the strain-gage balance. Secondly, the three components of $\mathbf{V}_{\text{wind}}$ are also zero, as the MAV is not immersed in an external airflow which could be produced by a wind tunnel. Finally, knowing that $[\mathbf{f}_{\text{body}}]_{\mathbf{z}_b} > 0$ as $[\mathbf{V}_{\text{prop}}]_{\mathbf{z}_b} > 0$ (see Eq. 42), $[\mathbf{f}_{\text{body}}]_{\mathbf{z}_b}$ could be rewritten as:

$$\begin{aligned}[\mathbf{f}_{\text{body}}]_{\mathbf{z}_b} &= \frac{1}{2}\rho S_s C_z \mathbf{V}_{wz} \sqrt{\mathbf{V}_{ux}^2 + \mathbf{V}_{vy}^2 + \mathbf{V}_{wz}^2} \\ &= \frac{1}{2}\rho S_s C_z [\mathbf{V}_{\text{prop}}]_{\mathbf{z}_b}^2.\end{aligned} \tag{60}$$

Thus, Eqs. 50, 51 and 52 are rewritten as follows:

$$X = -\beta \sin \delta_{c_y} \cos \delta_{c_x} \Omega_2^2, \tag{61}$$

$$Y = -\beta \sin \delta_{c_x} \Omega_2^2, \tag{62}$$

$$\begin{aligned}Z = {} & \sigma\alpha\Omega_1^2 + \sigma\beta \cos \delta_{c_x} \cos \delta_{c_y} \Omega_2^2 \\ & + \frac{1}{2}\rho S_s C_z \left(\frac{-2\sigma \left(\alpha\Omega_1^2 + \beta \cos \delta_{c_x} \cos \delta_{c_y} \Omega_2^2\right)}{\rho S_{\text{prop}}} \right).\end{aligned} \tag{63}$$

From Eqs. 57–59 and 61–63 which constitute the simplified form of the aerodynamic model, only Eq. 63 is nonlinear in the parameter space. To linearize the latter, it is assumed that:

$$C_{z\alpha} = C_z \alpha, \tag{64}$$

$$C_{z\beta} = C_z \beta. \tag{65}$$

Thus the aerodynamic loss parameter σ can be expressed as a function of Ω_1 and Ω_2. In order to find it, the α and β thrust aerodynamic coefficients must first be determined by: measuring the independent thrusts of each rotor with $\delta_{c_x} = 0$ and $\delta_{c_y} = 0$; assuming that the C_z value is known and approximated by a value found in the literature [22]; knowing that $\sigma = 1$ when $(\Omega_1 = 0, \Omega_2 \neq 0)$ or $(\Omega_1 \neq 0, \Omega_2 = 0)$. Thus α and β are the only unknown parameters from Eq. 63 which could be calculated separately. The values of α and β calculated here are used for the zero tilt angles of the cyclic swashplate. In the following, these two parameters will be identified by considering the whole range of variation of δ_{c_x}, δ_{c_y}, Ω_1 and Ω_2. To calculate $\bar{Z} = Z - \sigma\alpha\Omega_1^2$, the α parameter is supposed to be known from the coaxial rotot thrust map previously determined, when $\delta_{c_x} = 0$ and $\delta_{c_y} = 0$. From experiment, the value of α when $\delta_{c_x} = 0$ and $\delta_{c_y} = 0$ does not differ a lot when $\delta_{c_x} \neq 0$ and $\delta_{c_y} \neq 0$. This can be verified by calculating α through Eq. 64 after identifying the parameter vector Θ_k.

Now that the α and β values are known from the measured coaxial rotor thrust map, σ can be calculated for a certain region $\{\Omega_1,\Omega_2\}$ defined in Fig. 8. The resulting approximation values of σ are shown in Fig. 9. The aerodynamic loss efficiency is greatest when $\Omega_1 = \Omega_2$ and is about 10% of the theoretical maximum thrust. In the following, the interpolation function between σ and Ω_1, Ω_2 will be used, and it will also be assumed that $\sigma = \sigma(\Omega_1, \Omega_2)$. Under the hypothesis that u, v, w and $[\mathbf{V}_{\text{wind}}]$ are zero, $[\mathbf{f}_{\text{body}}]_{\mathbf{z}_b} > 0$, $C_{z\alpha} = C_z\alpha$, $C_{z\beta} = C_z\beta$ and the σ parameter is known, the simplified and linearized aerodynamic model can be locally written in the parameter space, where the index k corresponds to the measured sample number, Θ_k is the aerodynamic parameter vector, $\mathbf{w}_k$ is the process noise vector which is assumed to be zero,

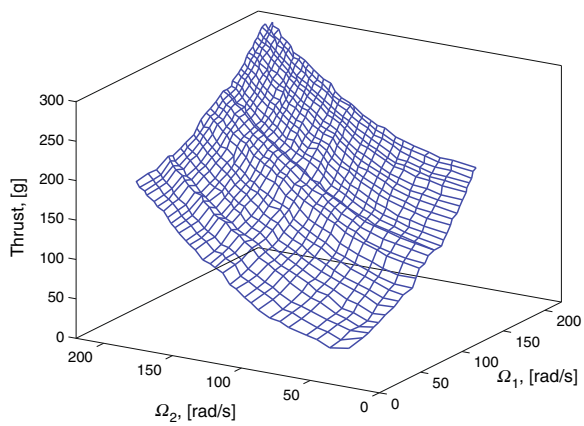

Fig. 8 Coaxial rotor thrust map

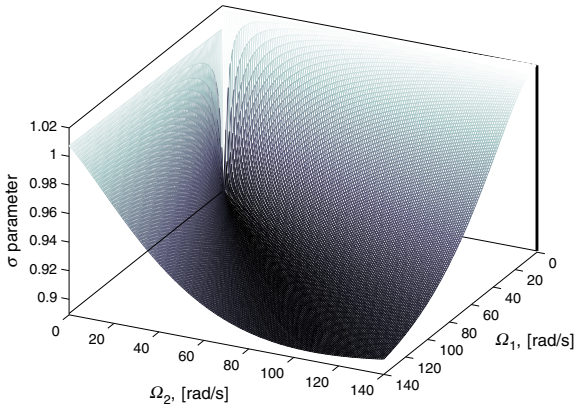

Fig. 9 σ approximation function

$\mathbf{z}_k$ the vector of input-output data, $\mathbf{X}_k$ the output matrix, and $\mathbf{v}_k$ the measurement noise vector, such that:

$$\Theta_{k+1} = \Theta_k + \mathbf{w}_k, \tag{66}$$

and

$$\mathbf{z}_k = \mathbf{X}_k \Theta_k + \mathbf{v}_k. \tag{67}$$

By computing Eqs. 57–65, the developed expressions of Eqs. 66 and 67 are written as:

$$\begin{aligned}&\left(\beta\ C_{z\alpha}\ C_{z\beta}\ \gamma_1\ \gamma_2\right)_{k+1}^{\top} \\ &\quad = \left(\beta\ C_{z\alpha}\ C_{z\beta}\ \gamma_1\ \gamma_2\right)_{k}^{\top} + \mathbf{w}_k^{\top},\end{aligned} \tag{68}$$

and

$$\begin{pmatrix} X \\ Y \\ \bar{Z} \\ L \\ M \\ N \end{pmatrix}_k = \begin{pmatrix} X_{11} & 0 & 0 & 0 & 0 \\ X_{21} & 0 & 0 & 0 & 0 \\ X_{31} & X_{32} & X_{33} & 0 & 0 \\ X_{41} & 0 & 0 & 0 & 0 \\ X_{51} & 0 & 0 & 0 & 0 \\ 0 & 0 & 0 & X_{64} & X_{65} \end{pmatrix}_k \begin{pmatrix} \beta \\ C_{z\alpha} \\ C_{z\beta} \\ \gamma_1 \\ \gamma_2 \end{pmatrix}_k + \mathbf{v}_k. \tag{69}$$

where

$$\begin{aligned}
\bar{Z} &= Z - \sigma\alpha\Omega_1^2, \\
X_{11} &= -\sin\delta_{c_y}\cos\delta_{c_x}\Omega_2^2, \\
X_{21} &= -\sin\delta_{c_x}\Omega_2^2, \\
X_{31} &= \sigma\cos\delta_{c_y}\cos\delta_{c_x}\Omega_2^2, \\
X_{32} &= \frac{-\sigma S_s}{S_{prop}}\Omega_1^2, \\
X_{33} &= \frac{-\sigma S_s}{S_{prop}}\cos\delta_{c_y}\cos\delta_{c_x}\Omega_2^2, \\
X_{41} &= -d\sin\delta_{c_x}\Omega_2^2, \\
X_{51} &= d\sin\delta_{c_y}\cos\delta_{c_x}\Omega_2^2, \\
X_{64} &= \Omega_1^2, \\
X_{65} &= \Omega_2^2.
\end{aligned} \tag{70}$$

Lemma 1 *Assume that there exist* $\xi \neq \zeta \leq N_s$ *and* $\lambda \neq \nu \leq N_s$ *such that the following conditions are verified:*

$$\begin{aligned}&\Omega_1^2(\xi)\Omega_2^2(\zeta)\cos\delta_{c_y}(\zeta)\cos\delta_{c_x}(\zeta) \\ &\quad \neq \Omega_1^2(\zeta)\Omega_2^2(\xi)\cos\delta_{c_y}(\xi)\cos\delta_{c_x}(\xi)\end{aligned} \tag{71}$$

and

$$\Omega_1^2(\lambda)\Omega_2^2(\nu) \neq \Omega_1^2(\nu)\Omega_2^2(\lambda), \tag{72}$$

where N_s *is the total measured sample number and* $\Omega_1(k)$, $\Omega_2(k)$, $\delta_{c_x}(k)$ *and* $\delta_{c_y}(k)$ *are the values of* Ω_1, Ω_2, δ_{c_x} *and* δ_{c_y} *at the sample time k. Then the aerodynamic model composed by the Eqs. 66 and 67 is sufficiently excited to identify the aerodynamic parameters.*

In order to ensure a sufficient number of measurements in the identification process, the persistently exciting condition must be previously verified, that is:

$$\epsilon \mathrm{I} \leq \sum_{k=1}^{N_s} \mathbf{Y}_k^{\top}\mathbf{Y}_k \leq \mu \mathrm{I}, \tag{73}$$

where ϵ and μ are positive reals, and I is the identity matrix. The persistently exciting condition 73 can be rewritten as:

$$\epsilon \mathrm{I} \leq \sum_{k=1}^{N_s} \mathbf{X}_k^{\top}\mathbf{X}_k = \mathbf{Y}^{\top}\mathbf{Y} \leq \mu \mathrm{I} \tag{74}$$

with $\mathbf{Y}^{\top} = \left[\mathbf{X}_1^{\top} \ldots \mathbf{X}_k^{\top}\ \mathbf{X}_{k+1}^{\top} \ldots \mathbf{X}_N^{\top}\right] \in \mathbb{R}^{5\mathrm{x}6N_s}$.

The condition 74 is fulfilled if and only if $\mathbf{Y}^\top$ is full row rank. Let $\mathbf{L}_i$ denotes the ith row of $\mathbf{Y}^\top$. The rows $\mathbf{L}_1$, and the grouped rows $\mathbf{L}_2 - \mathbf{L}_3$ and $\mathbf{L}_4 - \mathbf{L}_5$ are linearly independent of each other. The rows $\mathbf{L}_2$ and $\mathbf{L}_3$ are linearly indenpendent if there exist two sampled times $\xi \leq N_\mathrm{s}$ and $\zeta \leq N_\mathrm{s}$ with $\xi \neq \zeta$ such that:

$$\det \begin{bmatrix} \zeta_1 & \xi_1 \\ \zeta_2 & \xi_2 \end{bmatrix} \neq 0, \tag{75}$$

where

$$\begin{aligned} \zeta_1 &= \frac{-\sigma S_\mathrm{s}}{S_\mathrm{prop}} \Omega_1^2(\zeta), \\ \xi_1 &= \frac{-\sigma S_\mathrm{s}}{S_\mathrm{prop}} \Omega_1^2(\xi), \\ \zeta_2 &= \frac{-\sigma S_\mathrm{s}}{S_\mathrm{prop}} \cos\delta_{\mathrm{c}_y}(\zeta) \cos\delta_{\mathrm{c}_x}(\zeta) \Omega_2^2(\zeta), \\ \xi_2 &= \frac{-\sigma S_\mathrm{s}}{S_\mathrm{prop}} \cos\delta_{\mathrm{c}_y}(\xi) \cos\delta_{\mathrm{c}_x}(\xi) \Omega_2^2(\xi), \end{aligned} \tag{76}$$

which leads to

$$\begin{aligned} &\Omega_1^2(\xi)\Omega_2^2(\zeta) \cos\delta_{\mathrm{c}_y}(\zeta) \cos\delta_{\mathrm{c}_x}(\zeta) \\ &\quad \neq \Omega_1^2(\zeta)\Omega_2^2(\xi) \cos\delta_{\mathrm{c}_y}(\xi) \cos\delta_{\mathrm{c}_x}(\xi). \end{aligned} \tag{77}$$

The rows $\mathbf{L}_4$ and $\mathbf{L}_5$ are linearly independent if there exist $\lambda \leq N_\mathrm{s}$ and $\nu \leq N_\mathrm{s}$ with $\lambda \neq \nu$ such that:

$$\det \begin{bmatrix} \Omega_1^2(\nu) & \Omega_1^2(\lambda) \\ \Omega_2^2(\nu) & \Omega_2^2(\lambda) \end{bmatrix} \neq 0, \tag{78}$$

which is equivalent to

$$\Omega_1^2(\nu)\Omega_2^2(\lambda) \neq \Omega_1^2(\lambda)\Omega_2^2(\nu). \tag{79}$$

Thus the system can be identified if the conditions 77 and 79 are verified. This ends the proof of Lemma 1. Notice that experimentally, these conditions become true from a certain value of N_s.

The final purpose is to use the Kalman filter [12, 14, 17] method to obtain the parameter estimate values from the aerodynamic model described by the Eqs. 68–69 and the input-output measured data. This filter requires the calculation, at each step k, of the optimal Kalman gain $\mathbf{K}_k$, of the updated parameter estimate vector $\hat{\Theta}_k$, and of the updated estimate covariance matrix $\mathbf{P}_k$, such that:

$$\mathbf{K}_k = \mathbf{P}_k \mathbf{X}_k^\top \left[\mathbf{X}_k \mathbf{P}_k \mathbf{X}_k^\top + \mathbf{R}_k\right]^{-1}, \tag{80}$$

$$\hat{\mathbf{\Theta}}_k = \hat{\mathbf{\Theta}}_{k-1} + \mathbf{K}_k \left[\mathbf{z}_k - \mathbf{X}_k \hat{\mathbf{\Theta}}_{k-1}\right], \tag{81}$$

$$\mathbf{P}_k = \mathbf{P}_{k-1} - \mathbf{K}_k \mathbf{X}_k \mathbf{P}_{k-1} + \mathbf{Q}_k, \tag{82}$$

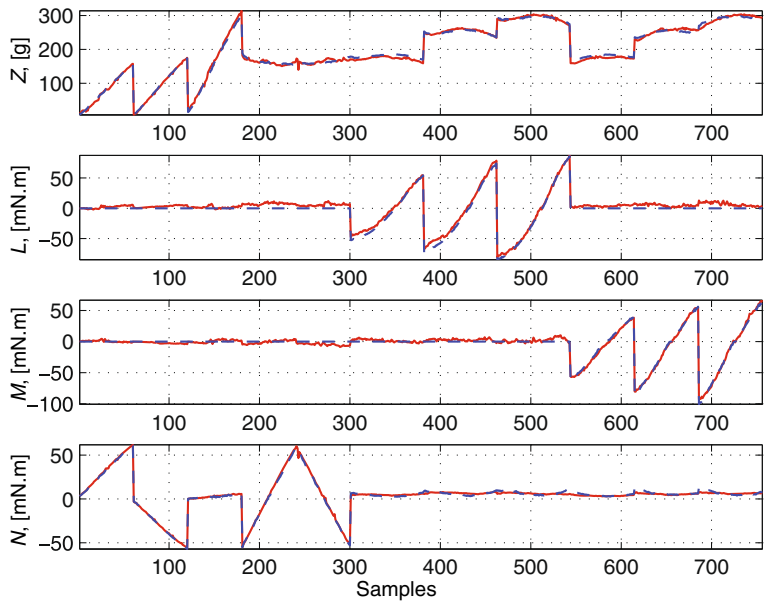

Fig. 10 Estimation—the *dashed lines* represent model outputs—the *solid lines* indicate the measured loads

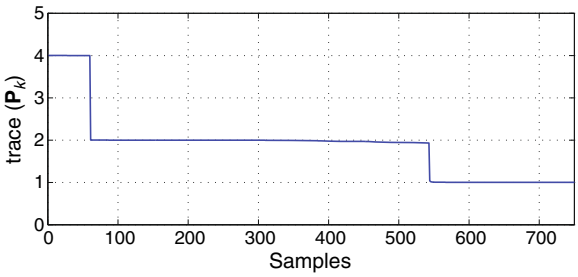

Fig. 11 Trace($\mathbf{P}_k$)

where $\mathbf{Q}_k$ and $\mathbf{R}_k$ are the process and measurement noise covariance matrices, respectively defined as:

$$\mathbf{Q}_k \triangleq \mathbb{E}\left[\mathbf{w}_k \mathbf{w}_k^\top\right] \quad \text{and} \quad \mathbf{R}_k \triangleq \mathbb{E}\left[\mathbf{v}_k \mathbf{v}_k^\top\right]. \tag{83}$$

The measurement noise $\mathbf{v}_k$ should not be neglected as it is generated by:

- The vibrations on the whole MAV aerodynamic balance structure due to the rotating rotors;
- The electronic acquisition chain;
- The strain-gage sensors.

Thus the diagonal elements of the measurement error covariance matrix $\mathbf{R}_k$ which must have a zero mean, be uncorrelated and have a constant variance, are calculated from the measured data, such that:

$$\text{diag}(\mathbf{R}_k) = \left(0.062\ 2.3\text{e}^{-5}\ 0.98\ 0.88\ 2.3\text{e}^{-5}\right). \tag{84}$$

The diagonal element values of $\mathbf{R}_k$ are calculated from the measured load signals, as the load values must be constant for each given input. Then the variance can be calculated by knowing the average calculated value of the output load signal. As shown by the estimation results in Fig. 10, the optimal parameter estimates are found by using the Kalman filter, which means that $\hat{\boldsymbol{\Theta}}$ converges to a fixed value. Those parameter estimate values are then reintroduced in the aerodynamic model to reconstruct the model outputs, in order to compare this output with the measured data, given the same input. The average error between the measured and model data corresponds to a relative error of about 3% for the forces and 6% for the moments, and the maximum relative error is of about 10% for the forces and for the moments, which is acceptable. For reasons of confidentiality, the aerodynamic parameter values are not shown. Nevertheless, the trace successive values of the $\mathbf{P}_k$ matrix below show the rapid convergence of the Kalman filter applied to our parameter estimation problem, as the input signals are rich enough, which implies that the condition from Eq. 73 has

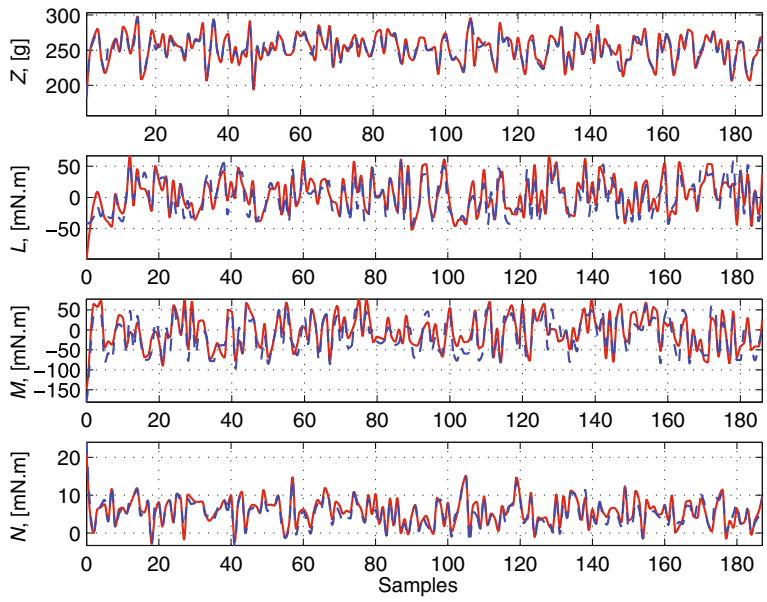

Fig. 12 Validation—the *dashed lines* represent the model outputs—the *solid lines* indicate the measured loads

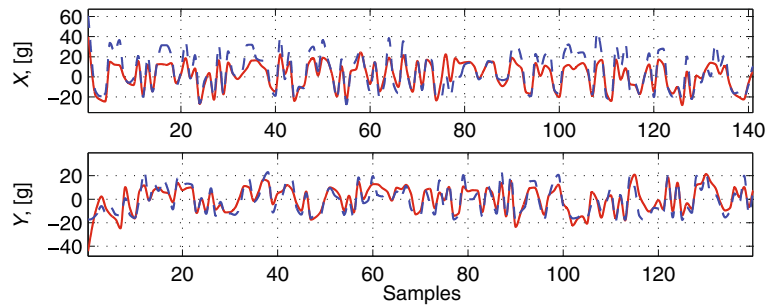

Fig. 13 Reconstruction—the *dashed lines* represent the model outputs—the *solid lines* stand for the measured loads

been previously verified. Indeed, Fig. 11 clearly shows that the gap between $\hat{\mathbf{\Theta}}_{k-1}$ and $\hat{\mathbf{\Theta}}_k$ is reduced to almost nothing (i.e. the final value of the trace($\mathbf{P}_k$) is amounts approximately to 1). Thus the final value of $\hat{\mathbf{\Theta}}$ is the optimal value.

5 Model Validation

Given that the aerodynamic parameters are known for the hover-flight case, the purpose is now to validate the model with its parameter values by comparing the model outputs with other sets of input-output measured data such as those used in the estimation step (in Section 4). According to Fig. 12, the aerodynamic system is well validated in hover conditions without any wind disturbances and only by using a linear estimation method, as the measured data fit the model outputs well. The main difficulty of the system identification, from the modeling to the validation step, is that the model must be rich enough to capture the main aerodynamic effects and simple enough for the future control law development work. This work has succeeded in this for the GLMAV identification in hover and near-hover flight conditions. To close this Section, two remarks can be made:

- The measurements used for the validation step were also used successfully for the estimation step, and conversely for the measurements presented in Section 4;
- According to Fig. 13, the forces X and Y were also well validated, although their measurements were not used in the estimation step.

6 Conclusions

In this paper the nonlinear modeling of a new Gun Launched MAV concept using two-bladed coaxial contra-rotating rotors was detailed for the hover-flight case. An experimental design using a strain-gage aerodynamic balance was proposed to collect measured input and output load data. Some simplifications brought to the nonlinear model led to a linearized aerodynamic submodel used for parameter identification. The persistently exciting condition was given in terms of physical variables of the GLMAV through two simple expressions, which was verified before the identification process. The aerodynamic parameters were also estimated using the Kalman filter linear estimation technique, from the aerodynamic submodel and using input-output data sets. Finally, the linear aerodynamic submodel was validated by comparisons between the model output reconstructions and other sets of data than those used in the estimation step, given to the same inputs.

Fig. 14 Embedded electronics

Fig. 15 Rotating coaxial rotor with lateral wind disturbances from the wind tunnel

In a future work, the purpose will be to develop input control laws for the hover-flight [27] case and autonomous trajectory tracking. In parallel to this work, we will use online or offline system identification processes including the 6-DoF model [8, 13] (i.e. with the active embedded electronics [8] shown in Fig. 14). Thereby, the system identification procedure will capture the GLMAV dynamics and will be compared to the identification method used in this paper. The wind disturbances will be considered to be data inputs in the parameter estimation task and will be generated by a subsonic wind tunnel during experiments, as shown in Fig. 15. Then a nonlinear estimation method like the extended Kalman filter will be used for the system identification.

Acknowledgements A. Koehl thanks J. Juncker and M. Dehaut for the realization of the electronic part and D. Bidino, M. Meister, and D. Willme for the GLMAV archetype mechanical design. This work is supported by the French National Centre for Scientific Research, the **ANR**, under the number **ANR 09 SECU 12**.

References

1. Ahmad, S.M., Chipperfield, A.J., Tokhi, M.O.: Modelling and control of a twin rotor multi-input multi-output system. In: Proceedings of the American Control Conference, pp. 1720–1724. AACC, Chicago (2000)
2. Bhandari, S., Colgren, R.: 6-dof dynamic model for a raptor 50 UAV helicopter including stabilizer bar dynamics. In: Proceedings of AIAA Modeling and Simulation Technologies Conference and Exhibit. AIAA, Keystone (2006)
3. Cai, G., Cai, A.K., Chen, B.M., Lee, T.H.: Construction, modeling and control of a mini autonomous UAV helicopter. In: Proceedings of the IEEE International Conference on Automation and Logistics. IEEE, Qingdao (2008)
4. Castillo, P., Lozano, R., Dzul, A.E.: Modelling and Control of Mini-flying Machines. Springer Advances in Industrial Control (2005)
5. Cerro, J.D., Valero, J., Vidal, J., Barrientos, A.: Modeling and identification of a small unmanned helicopter. In: Proceedings of IEEE Automation Congress, pp. 461–466. IEEE, Seville (2004)
6. Cunha, R., Silvestre, C.: Dynamic modeling and stability analysis of model-scale helicopters with Bell–Hiller stabilizing bar. In: Proceedings of AIAA Guidance, Navigation and Control Conference and Exhibit. AIAA, Austin (2003)
7. Ganguli, R.: Survey of recent developments in rotorcraft design optimization. J. Aircr. **441**(3), 493–510 (2004)
8. Garratt, M., Ahmed, B., Pota, H.R.: Platform enhancements and system identification for control of an unmanned helicopter. In: Proceedings of the 9th International Conference on Control, Automation, Robotics and Vision. IEEE, Singapore (2008)
9. Gnemmi, P., Haertig, J.: Concept of a gun launched micro air vehicle. In: Proceedings of 26th AIAA Applied Aerodynamics Conference. AIAA, Honolulu (2008)
10. Gnemmi, P., Koehl, A., Martinez, B., Changey, S., Theodoulis, S.: Modeling and control of two GLMAV hover-flight concepts. European Micro Aerial Vehicle Conference and Flight Competition. French-German Reasearch Institute of Saint-Louis, Delft (2009)
11. Hall, A.P.K., Wong, K.C., Auld, D.: Coaxial aeromechanical analysis of MAV rotorcraft with rotor interaction for optimisation. In: Proceedings of 12th AIAA/ISSMO Multidisciplinary Analysis and Optimization Conference. AIAA, Victoria (2008)
12. Jategaonkar, R.V.: Flight Vehicle System Identification: A Time Domain Methodology. AIAA Progress in Astronautics and Aeronautics (2006)
13. Kirschstein, S., Alles, W.: Parameter identification with a controlled free flying model of a spaceplane. Aerosp. Sci. Technol. **9**(4), 348–356 (2005)
14. Klein, V., Morelli, E.A.: Aircraft System Identification Theory and Practice. AIAA Education Series (2006)
15. Koehl, A., Rafaralahy, H., Martinez, B., Boutayeb, M.: Modeling and identification of a launched micro air vehicle: design and experimental results. In: AIAA Modeling and Simulation Technologies Conference and Exhibit, AIAA/MST, Toronto (2010)
16. Krashanitsa, R., Platanitis, G., Silin, B., Shkarayev, S.: Aerodynamics and controls design for autonomous micro air vehicles. In: Proceedings of AIAA Atmospheric Flight Mechanics Conference and Exhibit. AIAA, Keystone (2006)
17. Leith, D.J.: Identification of the SA-330 Puma helicopter. IEE Proc. Control Theory Appl. **141**(2), 130–136 (1994)
18. Mettler, B.: Identification Modeling and Characteristics of Miniature Rotorcraft. Kluwer Academic Publishers (2003)
19. Pflimlin, J.M.: Commande d'un Minidrone à Hélice Carénée: De la Stabilisation dans le Vent à la

Navigation Autonome. Ph.D. thesis, Ecole Doctorale Systèmes, Laboratoire d'Analyse et d'Architecture des Systèmes, Toulouse (2006)
20. Pines, D.J., Bohorquez, F.: Challenges facing future micro-air-vehicle development. J. Aircr. **43**(2), 290–305 (2006)
21. Ramasamy, M., Lee, T.E., Leishman, J.G.: Flowfield of a rotating-wing micro air vehicle. J. Aircr. **44**(4), 1236–1244 (1994)
22. Rebuffet, P.: Aérodynamique Expérimentale. Béranger-Dunod (1950)
23. Smith, T.R., Shook, L., Uhelsky, F., McCoy, E., Krasinski, M., Limaye, S.: Ballute and parachute decelerators for FASM/QUICKLOOK UAV. In: Proceedings of Aerodynamic Decelerator Systems Technology Conference and Seminar. AIAA, Monterey (2003)
24. Taylor, D., Ol, M., Cord, T.: SkyTote advanced cargo delivery system. In: AIAA/ICAS International Air and Space Symposium and Exposition: The Next 100 Years. AIAA, Dayton (2003)
25. Valvanis, K.P.: Advances in Unmanned Aerial Vehicles State of the Art and the Road to Autonomy. Springer (2007)
26. Walchko, K.J., Nechyba, M.C., Schwartz, E., Arroyo, A.: Embedded Low Cost Inertial Navigation System. Florida Conference on Recent Advances in Robotics, University of Florida, Dania Beach (2003)
27. Wang, H., Wang, D., Niu, X.: Modeling and hover control of a novel unmanned coaxial rotor/ducted-fan helicopter. In: Proceedings of the IEEE International Conference on Automation and Logistics. IEEE, Jinan (2007)
28. Wereley, N.M., Pines, D.J.: Feasibility Study of a Smart Submunition: Deployment From a Conventional Weapon. ARL-CR-0475, Army Research Laboratory, Aberdeen Proving Ground (2001)